第 49 卷 第 22 期/2022 年 11 月/中国激光 研究论文

中国激光

单晶锗激光电解自耦合协同加工基础研究

王超，朱浩*，张朝阳，蒋子宣，杜文武，张敏

江苏大学机械工程学院，江苏 镇江 212013

摘要 以硅、锗为代表的半导体材料在集成电路芯片、微机电系统等领域得到了广泛应用。针对该类材料硬脆性强、传统加工工艺难以加工的不足，提出了一种激光电化学复合加工方法，利用皮秒激光辐照定域以提高单晶锗的电导率，实现了激光热力效应与电化学阳极溶解的自耦合协同加工。阐述了该加工方法的理论依据，设计了背向光控电解试验，进行了机理验证，分析了光控电解所得的凹坑结构的形貌特征，讨论了偏置距离对其的影响规律。在此基础上，将激光热力效应与电化学阳极溶解耦合于单晶锗上表面，开展了激光电解自耦合协同微切槽试验，分析了微槽加工表面的特点，讨论了加工电压对微沟槽尺寸的影响规律。

关键词 激光技术；自耦合协同加工；激光电解；单晶锗；表面形貌

中图分类号 TN249 **文献标志码** A **DOI**：10.3788/CJL202249.2202019

1 引 言

硅、锗等材料被视为半导体行业的基石，被广泛应用于芯片、光伏、医疗器械、微机电系统等领域[1-2]。在硅、锗上加工出特定形貌的微细结构可以实现多种功能，如增强表面抗反光性能[3]、调控材料亲疏水特性[4]，进而制备出微凹透镜阵列[5]、液滴自驱动结构等[6]。以硅和锗为代表的半导体材料有着良好的结构与功能属性，但受制于其高脆性与低断裂韧度，材料的可加工性较差[7]，微加工难度较高。得益于国内外科研机构多年的探索，该类材料的微加工研究已取得可喜进展，目前主要有微车削/铣削加工、光刻加工、电解加工、激光加工、化学刻蚀加工等。上述加工方法各有特色，适用场合不同，也有各自的局限性。例如，采用微细端铣方式加工单晶硅时，为了避免在延展区域内产生裂纹，需要将单步进给量控制在 250 nm 以下，这导致材料的去除效率较低[8]；光刻加工工艺较为复杂，对光刻机等设备要求高，且不同种类、不同晶向的基体材料对腐蚀剂的要求不同[9-10]，故该方法适合稳定的规模化生产；采用电化学溶解方法时，受限于半导体材料特性，电流密度往往低于金属材料，导致加工效率较低[11]，且易生成钝化层，阻碍电解加工的持续进行。

激光加工具有柔性强、机械应力小、适用范围广等诸多优点[12-14]，已在硅、锗等半导体材料加工方面得到了大量应用。Kanaujia 等[15]采用超短脉冲激光，结合化学后处理的方式，制备出微通道、微金字塔等结构，通过试验探讨了工艺参数并进行了适当优化，但激光刻蚀会产生一些不理想结构，例如 V 形凹坑、重熔层和碎片。另外，Luong 等[16]采用超短脉冲激光在 KOH 溶液中刻蚀硅，结果显示，湿刻蚀过程中凹槽深度从 300 nm 增加到大约 6 μm，深度得到加深，同时均匀性也得到了保持。Zhang 等[17]验证了皮秒激光切割薄锗晶圆的可行性，在极薄锗晶圆上得到了高质量微槽结构，并指出辅助液体种类和激光参数对切割质量的影响显著。Pan 等[18]采用激光水射流复合加工方式，在单晶硅上开展了微切槽研究，探讨了工艺参数对沟槽深度、宽度和热影响区宽度的影响，结果表明，引入水射流可以显著减弱激光加工带来的热损伤。Zhu 等[19]以单晶锗为对象，开展了激光水射流复合切槽的研究，指出高压水射流可及时高效去除激光软化的材料，有效消除热累积导致的热损伤。为了进一步提高加工质量，相关学者将激光刻蚀与电化学加工结合，实现了半导体材料的微细加工。Yu 等[20]探索了电解加工对激光刻蚀表面质量的影响，指出电解加工的引入能提高材料去除率，同时获得良好的表面质量。

本文提出了一种激光电解自耦合协同加工方法，利用激光局域热效应与光激发产生的大量自由电子，定域提高了半导体材料的导电性能，进而提高了电解加工效率，同时借助电化学阳极溶解，从原子层面实现了材料去除，改善了激光加工表面的质量，获得了热损伤小、定域性强、表面质量好的加工结果。在该方法

收稿日期：2022-03-01；**修回日期**：2022-03-29；**录用日期**：2022-04-07

基金项目：国家自然科学基金(51905226，52075227)

通信作者：*haozhu@ujs.edu.cn

中，电解加工位置可由激光辐照决定，无需对刀步骤或特殊阴极设计，可实现激光电解自动耦合协同加工。

2 加工机理及试验验证

2.1 激光辐照定域增大单晶锗电导率的机理

激光辐照定域增大单晶锗电导率(A)的示意图如图 1 所示。皮秒激光辐照于微小区域内，在加工区域周边会产生显著高温区域，根据 Morin 等[21]的测试结果，单晶锗电导率随温度的升高将急剧增大，如图 1(b)所示。这是由于价带电子可从热振动晶格处吸收能量，转变为导带电子，因此材料内可自由移动的电子密度增大。同时，当入射激光的单光子能量大于禁带宽度(E_g)时，锗材直接吸收光子能量也可能引发电子发生跃迁，进一步增大自由电子密度。上述自由电子密度的增大机制都是由入射激光引发的，增大位置与激光辐照位置严格对应，激光未辐照处的电导率仍处于较弱水平。借助激光辐照，合理引入外部电场，有望实现光控定域电解加工。在本方法中，激光脉冲宽度不影响加工，但更短脉冲宽度有助于产生更集中的温度场，进而提高光控电解加工的定域性。

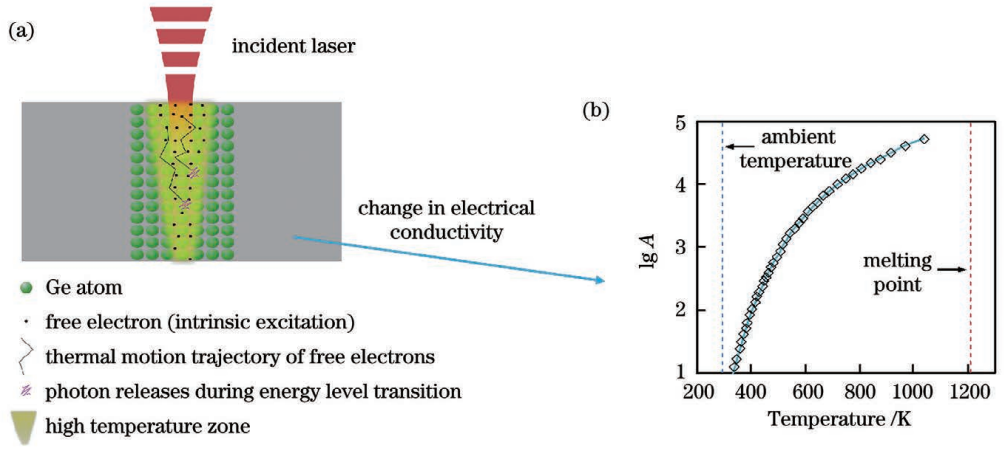

图 1 激光辐照定域增大单晶锗电导率的示意图。(a)入射激光作用于 Ge 晶格内部；(b)电导率随温度的变化曲线

Fig. 1 Schematics of localized enhancement of single crystal Ge electrical conductivity by laser irradiation. (a) Incident laser applied inside Ge lattice; (b) electrical conductivity versus temperature

2.2 验证方案与加工装置

光控定域电解加工试验方案示意图如图 2 所示，其中 AHLECM 表示自耦合协同激光电解加工。材料选用单晶锗，厚度为 500 μm。在锗材上表面进行激光辐照，合理调控激光参数，避免材料去除及相变，确保加工后上表面无任何可见变化。在下表面的正下方放置尺寸为 30 mm×30 mm×2 mm 的铜板作为阴极以引入均匀电场，采用中性硝酸钠电解液作射流，观察是否能产生定域电解加工效果。所涉及系统包括激光加工系统、控制系统、射流系统、加工位置系统。在激光

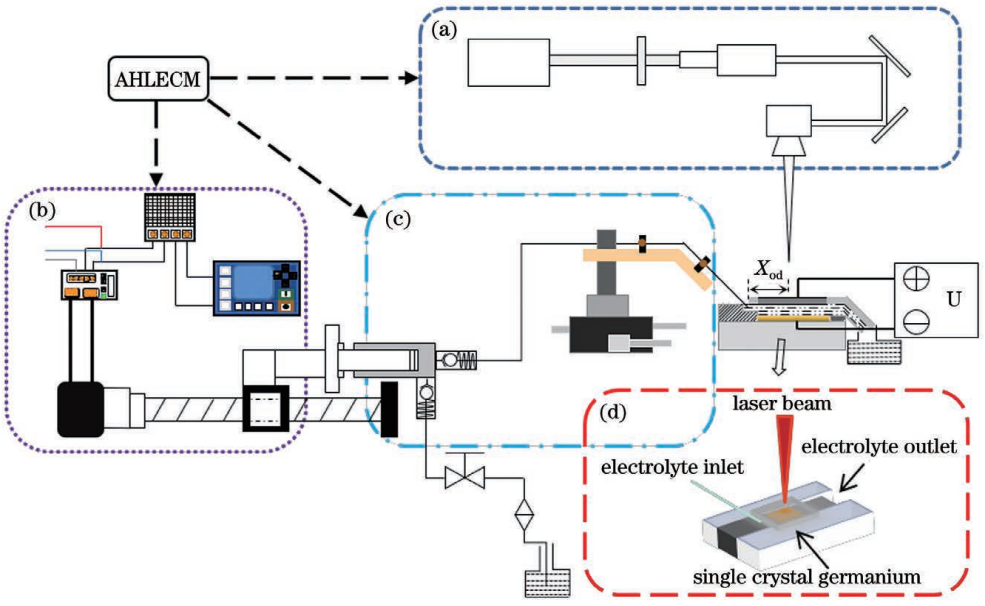

图 2 光控电解加工中的系统。(a)激光加工系统；(b)控制系统；(c)射流系统；(d)加工位置系统

Fig. 2 Systems in laser-controlled electrolytic processing. (a) Laser processing system; (b) control system; (c) jet system; (d) processing position system

加工系统中，使用波长为 1064 nm 的超短脉冲皮秒激光器，光斑理论直径为 20 μm，脉宽时间为～12 ps；在控制系统中，利用伺服电机、控制器等控制滚珠丝杠沿导轨运动，进而推动活塞杆前、后运动，实现电解液输出及补液；在射流系统中，射流针头位置通过支架被固定在 x-y-z 三向微调平台上，实现 0.03 mm 精度的进给，此处定义激光束焦点距射流针头的水平距离为偏置距离（X_{od}）；在加工位置系统中，材料被放在夹具装置上，射流从单晶锗背面的左边进、右边出，与阳极单晶锗晶圆的间距为 2 mm。

试验加工装置图如图 3 所示。激光实际输出功率为 4 W，重复频率为 0.2 MHz，离焦量为 12 mm，滚珠丝杠的进给速度为 50 mm/min，阴阳极的加工间隙为 2 mm，硝酸钠溶液浓度（质量分数，下同）为 10%，射流针头的固定角度为 45°，针头内径为 0.6 mm，电解液射流的出口速度为 3.85 m/s，有效加工时间总计 180 s，分三次进行，每次加工 60 s，间隔 10 s。

试验后对样件进行超声清洗，然后进行形貌检测。采用扫描电镜（SEM）分析加工表面的形貌特征，通过能谱仪（EDS）分析加工表面的元素含量，同时，利用激光拉曼光谱仪分析表面的结构成分。利用激光共聚焦

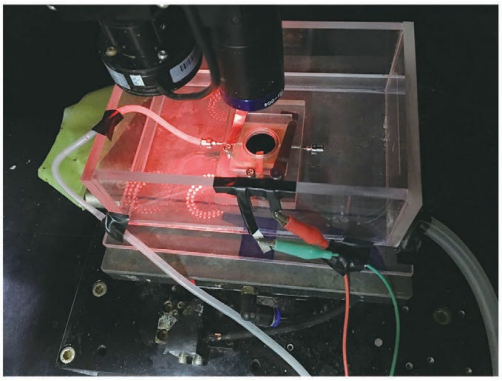

图 3　试验加工装置图

Fig. 3　Experimental processing device

显微镜得到凹坑结构的三维形貌。间隔 45°提取凹坑二维轮廓，如图 4（a）所示。基于提取的轮廓，按图 4（b）所示方法定义入口直径、深度数值、凹坑侧壁锥度，取四次测量数据的平均值作为测量读数。凹坑侧壁锥度 θ 的计算公式为

$$\theta=\arctan\left(\frac{2D}{D_{d}-d}\right),\tag{1}$$

式中：D_d 为入口直径；d 为凹坑轮廓的切线与底部交线的水平距离；D 为凹坑深度。

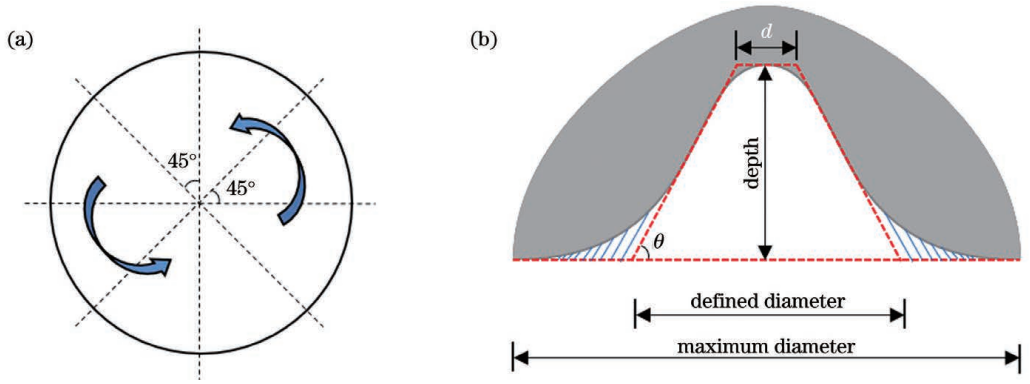

图 4　轮廓提取和参数定义示意图。（a）凹坑二维轮廓提取示意图；（b）凹坑参数定义示意图

Fig. 4　Diagrams of contour extraction and parameter definition. (a) Schematic of two-dimensional contour extraction from dimple; (b) diagram of dimple parameter definition

2.3　不同偏置距离的影响

采用给定的加工参数，当射流偏置距离逐渐增大时，所得的背部凹坑形貌如图 5 所示。背部凹坑中心与上表面激光入射位置严格对应，证明了激光辐照可在单晶锗材内诱导产生定域导电通道，电流优先通过，电流密度定域增大，因此更多的锗原子被电解去除。凹坑表面无热损伤、无微裂纹，凹坑底部平滑，边缘无材料堆积，呈现了典型的电解加工特征。但在图 5（c1）中也观测到了少许颗粒附着，其原因可能与偏置距离变化引发的流速变化相关。

对凹坑表面进行元素含量分析，如图 6 所示，对比无颗粒和有颗粒位置，发现两处都存在 O，但颗粒处的 O 含量明显高于 Ge。对所得表面进行拉曼光谱分析，如图 7 所示，观测到 300.4 cm^{-1} 和 448 cm^{-1} 两处峰，分别对应 Ge 和 GeO_2[22-23]。上述检测结果表明，光控电解加工至少在材料表面生成一种氧化产物 GeO_2，其可能对电解过程产生阻碍作用。

图 8（a）为不同偏置距离下的加工电流变化图，当引入激光辐照后，电流迅速增加，之后稳定在一定范围内，撤去激光后电流急剧下降至原始水平。上述变化可归因于激光辐照对单晶锗电导率的定域增大作用。此外，加工电流最大值出现在偏置距离约 9 mm 处。图 8（b）为不同偏置距离对各参数的影响规律，可见凹坑深度、入口直径、去除体积和凹坑侧壁锥度也都存在拐点，且最大值都在 7 mm 或者 9 mm 的偏置距离处取得。上述现象可能与偏置距离对传热传质两方面的影响有关。当偏置距离较小时，如 5 mm，加工位置距离射流出口近，加工区域的电解液流速大，冷却作用强，不利于电解减材，但同时较高的流速也促进了加工产物的排出，抑制了浓差极化；当偏置距离较大时，如

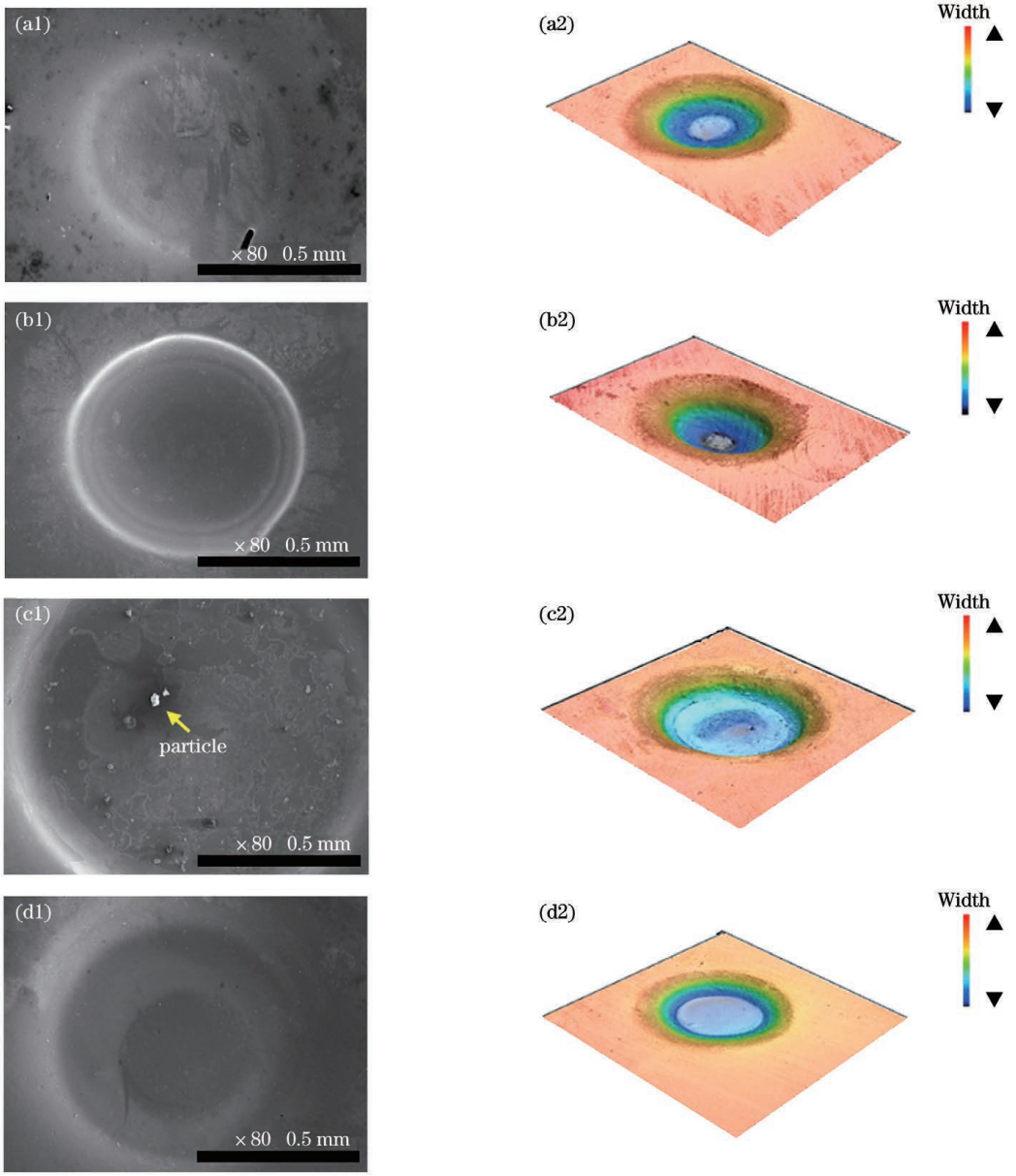

图 5 不同偏置距离下的凹坑形貌图。(a1)(a2)5 mm;(b1)(b2)7 mm;(c1)(c2)9 mm;(d1)(d2)11 mm

Fig. 5 Dimple morphologies under different offset distances. (a1)(a2) 5 mm; (b1)(b2) 7 mm; (c1)(c2) 9 mm; (d1)(d2) 11 mm

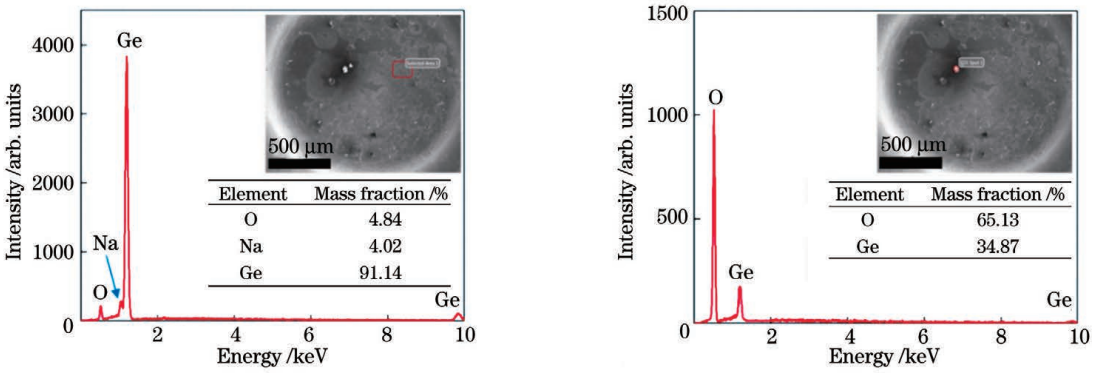

图 6 有无颗粒附着时的 EDS 分析结果。(a)无颗粒附着;(b)有颗粒附着

Fig. 6 EDS analysis results with and without particle attachment. (a) Without particle attachment; (b) with particle attachment

11 mm,加工位置距离射流出口远,加工区域的电解液射流流速低,冷却作用弱,但产物排出能力也减弱。传热与传质相互影响,共同决定了加工过程及结果。加工结果显示,随着偏置距离的增加,光控电解加工微坑开口的宽度整体呈增大趋势,并在 9 mm 偏置距离处取得最大值;微坑深度的变化平缓,在 7 mm 偏置距离

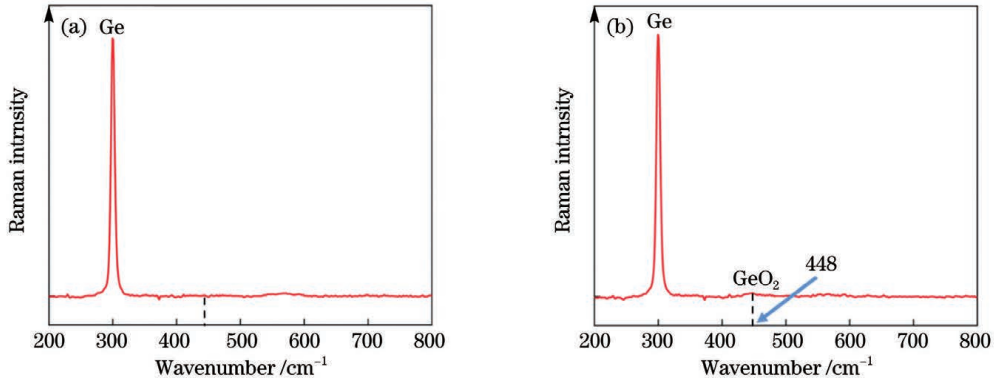

图 7 不同偏移距离下的 Raman 图。(a)7 mm;(b)9 mm

Fig. 7 Raman diagrams under different offset distances. (a) 7 mm; (b) 9 mm

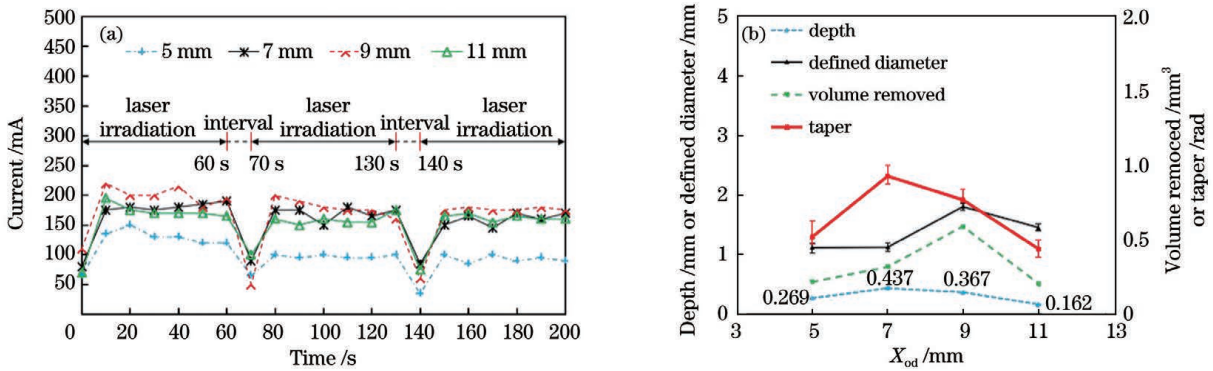

图 8 电流变化曲线图和加工结果。(a)不同偏置距离下测得的电流;(b)偏置距离对各参数的影响

Fig. 8 Current variation curves and machining results. (a) Measured currents under different offset distances; (b) effect of offset distance on each parameter

附近处取得最大值;微坑侧壁锥度先增大后减小,在 7 mm 偏置距离处取得最大值;材料去除量在 9 mm 偏置距离处取得最大值,与电流情况一致。

3 激光电解自耦合微切槽的初步试验研究

3.1 试验方案及装置

在验证了激光辐照可实现定域电解加工后,将激光辐照与电解作用耦合于材料上表面,如图 9 所示,实现激光电解自耦合协同微加工。利用激光刻蚀高效减材,利用电化学阳极溶解进一步提高材料表面质量,从而获得高质量加工表面。

激光电解自耦合协同加工系统如图 10 所示。以皮秒脉冲激光为光源,锗材底部连接脉冲电源正极,以上方导电玻璃(ITO)为阴极,射流电解液从阴阳极中间空隙流过。所用激光参数包括:激光实际输出功率为 7 W,重复频率为 0.2 MHz,扫描方式为单线多次加工,扫描长度为 10 mm,扫描速度为 1500 mm/s;加工电压参数包括:供电方式为平波稳压,频率为 1000 Hz,占空比为 50%,加工电压为 4 V;射流电解液参数包括:硝酸钠浓度(质量分数)为 10%,射流出口速度为 4 m/s;其他参数包括:加工时间为 2 min。图 10 所涉及装置的绝大部分与 2.2 节相同,不同处在于阴极选择、工件装夹定位方式等。

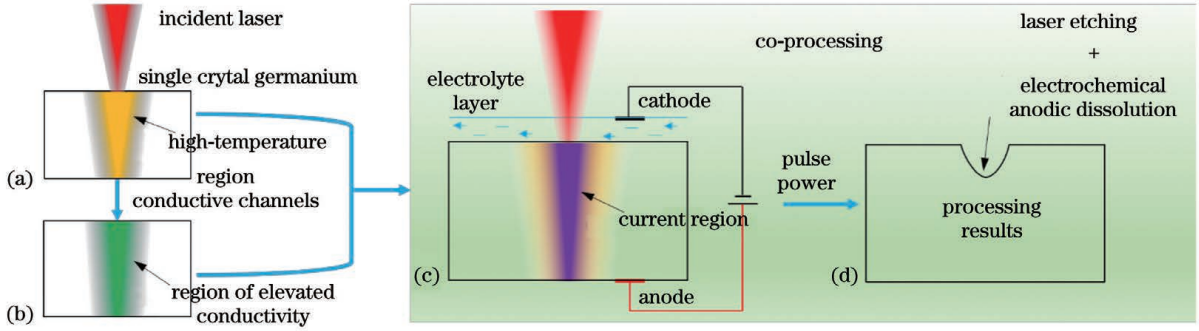

图 9 激光电解自耦合协同微加工过程。(a)高温区域;(b)电导率升高区域;(c)电流变化区域;(d)协同加工的结果

Fig. 9 Process of auto-coupled laser-electrochemical co-machining. (a) High temperature region; (b) region of elevated conductivity; (c) region of current change; (d) co-machining result

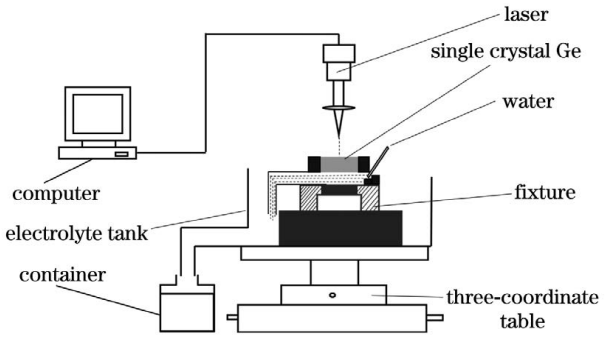

图 10 激光电解自耦合协同加工系统示意图

Fig. 10 Schematic of auto-coupled laser-electrochemical co-machining system

3.2 加工结果分析

分别进行激光干切加工、激光电解自耦合协同加工微切槽试验，所得结果如图 11 所示。在图 11(a)中，激光干切所得的微沟槽的两边缘热影响区较为明显，存在飞溅物和重铸层，加工过程中熔融态的材料向外喷出，而后冷却凝固堆积在边缘处，形成粗糙的边缘形貌。图 11(b)为相同条件下激光电解自耦合协同加工所得的微槽结构，图 11(c)为局部放大图，图 11(d)为 EDS 分析图。在相同激光参数下，引入电解加工后，微槽宽度明显增加，且两侧边缘较为平整，基本没有飞溅颗粒物附着；槽底存在微沟壑结构，微沟壑宽度小于 10 μm，结构整体沿微槽长度方向分布；微沟壑间存在凸起结构，其上分布有较为均匀的微米级颗粒物，EDS 分析结果显示其中以 Ge 为主，含有少量 O，可能与电解加工过程有关。在激光电解自耦合协同加工过程中，阴阳极间使用了带有流道的掩模板，其对电解液流速有限制作用，到达加工区域的电解液速度变小，可能影响产物去除；此外，激光穿过 ITO 玻璃和较厚的电解液层达到单晶锗材上，激光束在 ITO 玻璃及射流电解液中多次折射和反射，可能造成光斑分散，导致较大的微槽宽度。

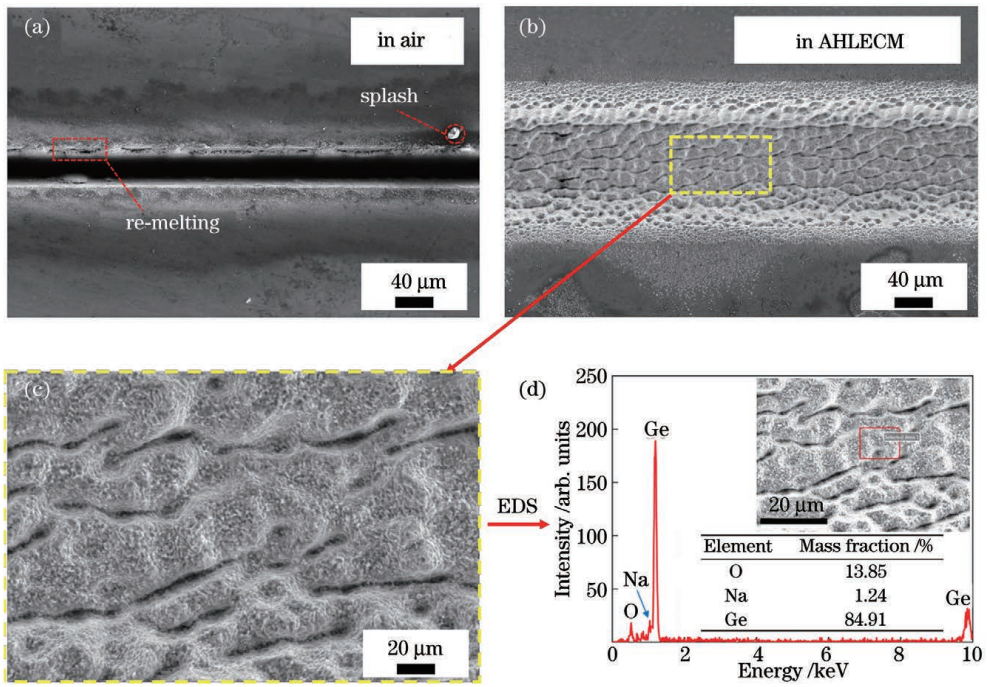

图 11 激光干切和激光电解自耦合协同加工所得的微沟槽。(a)激光干切；(b)激光电解自耦合协同加工；(c)SEM 表面形貌图；(d)EDS 分析结果

Fig. 11 Microgrooves by laser dry-cutting and auto-coupled laser-electrochemical co-machining. (a) Laser dry-cutting; (b) auto-coupled laser-electrochemical co-machining; (c) SEM surface morphology; (d) EDS analysis result

当加工电压从 1 V 增加到 4 V 时，激光电解自耦合协同加工所得的微沟槽三维形貌如图 12 所示，微槽尺寸测量值如表 1 所示。从图 12 中可以看出：微沟槽的剖面轮廓清晰，内壁较为平整光滑，整体形貌较好；随着加工电压从 1 V 增加到 4 V，槽宽不断变宽，深度逐渐加深，槽底逐渐开阔。主要原因在于，随着加工电压的增大，相同条件下电流密度增大，更多原子被电解去除，微槽深度、宽度逐渐增加。加工电压对加工结果的影响较为显著，尤其是在微槽宽度方面，进一步证明了电化学溶解是激光电解自耦合协同作用过程中的一个重要现象。

表 1 不同加工电压下的微切槽宽度和深度

Table 1 Microgroove widths and depths under different applied voltages

Applied voltage /V	Width /μm	Depth /μm
1	240.1	106.8
2	252.5	109.3
3	252.1	112.9
4	268.2	114.4

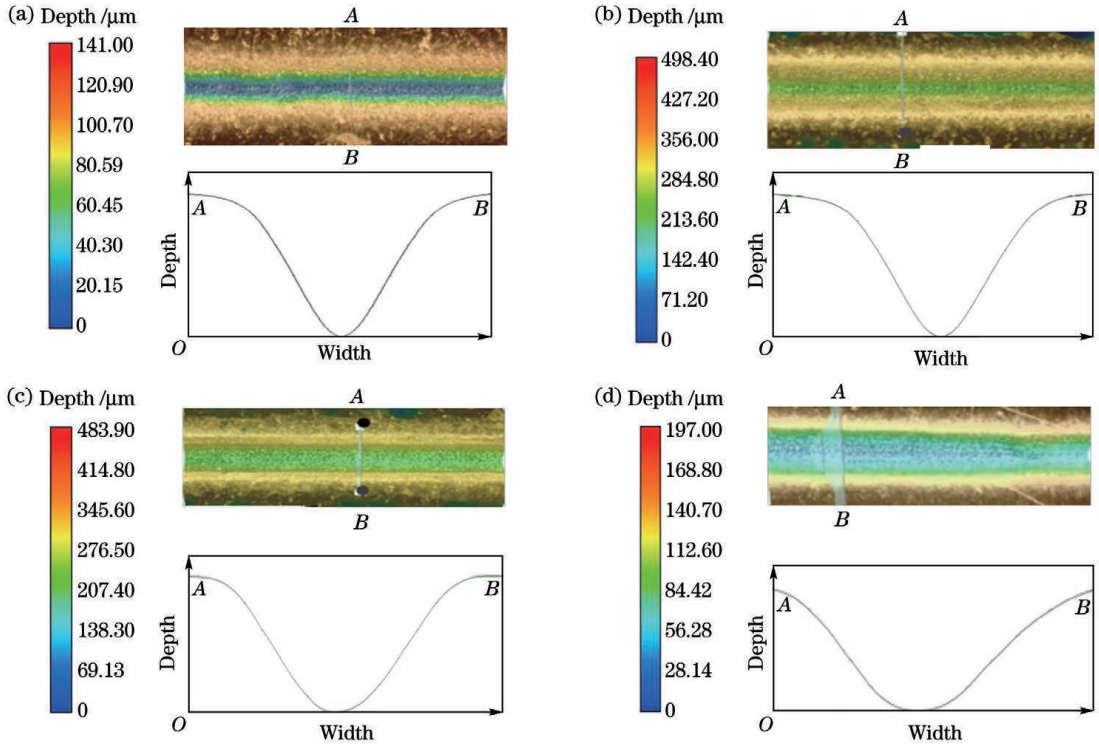

图 12 不同加工电压下的三维形貌图。(a)1 V;(b)2 V;(c)3 V;(d)4 V

Fig. 12 3D morphologies under different processing voltages. (a) 1 V; (b) 2 V; (c) 3 V; (d) 4 V

4 结 论

利用激光辐照在材料内产生定域导电通道,进而实现激光电解自耦合协同加工。设计了背向光控电解加工试验进行验证,当以中性硝酸钠溶液为电解液、水平铜片为阴极时,上表面激光辐照可在单晶锗背面引发定域电解,得到凹坑结构,且凹坑中心对应上表面激光辐照位置,同时引入的激光辐照可大幅增大加工电流。上述结果证明了激光辐照可定域增强材料的导电性能,引发定域电解加工,无需额外对刀步骤。

探讨了电解液射流偏置距离对凹坑形貌的影响规律。随着偏置距离的增加,最大加工电流、凹坑直径与深度、侧壁锥度、去除体积都先增大后减小,且拐点都在 7~9 mm 偏置距离附近处,从传热、传质两方面对不同偏置距离的影响进行了分析。

将激光刻蚀与电化学溶解耦合于同一作用位置,可实现激光电解自耦合协同加工,并据此开展了复合微切槽的初步试验研究。分析了所得微槽结构的形貌特点,研究了加工电压对微槽尺寸的影响规律,发现微槽深度、宽度都随加工电压的增加而增大,证明了电化学溶解是激光电解自耦合协同作用过程中的一个重要现象。

参 考 文 献

[1] 杨策, 程虎虎, 曲良体. 新型能源器件的激光微纳加工研究进展[J]. 中国激光, 2021, 48(15): 1502004.
Yang C, Cheng H H, Qu L T. Research advancement on laser micro-nano processing of new energy devices [J]. Chinese Journal of Lasers, 2021, 48(15): 1502004.

[2] 夏菁菁, 余俊, 王占山, 等. 单晶硅化学机械抛光划痕演变研究[J]. 光学学报, 2022, 42(9): 0912002.
Xia J J, Yu J, Wang Z S, et al. Scratch evolution for monocrystalline silicon during chemical-mechanical polishing[J]. Acta Optica Sinica, 2022, 42(9): 0912002.

[3] Vorobyev A Y, Guo C L. Antireflection effect of femtosecond laser-induced periodic surface structures on silicon[J]. Optics Express, 2011, 19(5): A1031-A1036.

[4] Ems H, Ndao S. Microstructure-alone induced transition from hydrophilic to hydrophobic wetting state on silicon[J]. Applied Surface Science, 2015, 339: 137-143.

[5] Liu X Q, Chen Q D, Guan K M, et al. Dry-etching-assisted femtosecond laser machining[J]. Laser & Photonics Reviews, 2017, 11(3): 1600115.

[6] 任英明, 张志宇. 双步激光辐射提升纳秒激光抛光单晶硅的表面[J]. 光学学报, 2022, 42(7): 0714004.
Ren Y M, Zhang Z Y. Surface of nanosecond laser polished single-crystal silicon improved by two-step laser irradiation[J]. Acta Optica Sinica, 2022, 42(7): 0714004.

[7] 刘志东, 邱明波, 汪炜, 等. 锗晶体放电加工特性及进电方式研究[J]. 机械工程学报, 2011, 47(5): 177-182.
Liu Z D, Qiu M B, Wang W, et al. Research on electrical discharge machining characteristics and mode of providing power of germanium crystal[J]. Journal of Mechanical Engineering, 2011, 47(5): 177-182.

[8] Arif M, Rahman M, San W Y. An experimental investigation into micro ball end-milling of silicon[J]. Journal of Manufacturing Processes, 2012, 14(1): 52-61.

[9] Leancu R, Moldovan N, Csepregi L, et al. Anisotropic etching of germanium[J]. Sensors and Actuators A: Physical, 1995, 46(1/2/3): 35-37.

[10] 陈骄, 董培涛, 邸荻, 等. TMAH 溶液中的(110)硅各向异性湿法腐蚀及其在不同添加剂下的腐蚀特性研究[J]. 传感技术学报, 2011, 24(2): 185-189.
Chen J, Dong P T, Di D, et al. Anisotropic wet etching behaviors and characteristics of(110)-oriented silicon in TMAH

solution with different surfactants [J]. Chinese Journal of Sensors and Actuators, 2011, 24(2): 185-189.
[11] Allongue P, Jiang P, Kirchner V, et al. Electrochemical micromachining of p-type silicon [J]. The Journal of Physical Chemistry B, 2004, 108(38): 14434-14439.
[12] Zhao W Q, Yu Z S. Self-cleaning effect in high quality percussion ablating of cooling hole by picosecond ultra-short pulse laser[J]. Optics and Lasers in Engineering, 2018, 105: 125-131.
[13] Wu T N, Wu Z P, He Y C, et al. Femtosecond laser textured porous nanowire structured glass for enhanced thermal imaging [J]. Chinese Optics Letters, 2022, 20(3): 033801.
[14] Yin K, Wu Z P, Wu J R, et al. Solar-driven thermal-wind synergistic effect on laser-textured superhydrophilic copper foam architectures for ultrahigh efficient vapor generation[J]. Applied Physics Letters, 2021, 118(21): 211905.
[15] Kanaujia P K, Bulbul A, Parmar V, et al. Ultrafast laser based hybrid methodology of silicon microstructure fabrication for optoelectronic applications [J]. Applied Surface Science, 2017, 420: 63-69.
[16] Luong K P, Tanabe-Yamagishi R, Yamada N, et al. Laser-assisted wet etching of silicon back surfaces using 1552 nm femtosecond laser[J]. International Journal of Electrical Machining, 2020, 25: 7-13.
[17] Zhang D S, Gökce B, Sommer S, et al. Debris-free rear-side picosecond laser ablation of thin germanium wafers in water with ethanol[J]. Applied Surface Science, 2016, 367: 222-230.
[18] Pan X N, Huang C Z, Wang J, et al. Laser-assisted waterjet micro-grooving of silicon wafers for minimizing heat affected zone[J]. Materials Science Forum, 2016, 861: 133-138.
[19] Zhu H, Wang J, Yao P, et al. Heat transfer and material ablation in hybrid laser-waterjet microgrooving of single crystalline germanium [J]. International Journal of Machine Tools and Manufacture, 2017, 116: 25-39.
[20] Yu P H, Wu K L, Lee S M, et al. Effect of voltage supply mode on electrolytic machining of polycrystalline silicon[J]. Materials and Manufacturing Processes, 2011, 26(12): 1459-1465.
[21] Morin F J, Maita J P. Conductivity and Hall effect in the intrinsic range of germanium [J]. Physical Review, 1954, 94 (6): 1525-1529.
[22] Geng R W, Yang X J, Xie Q M, et al. Fundamental study on material removal mechanism in single-crystal germanium [J]. Infrared Physics & Technology, 2021, 116: 103773.
[23] Arai N, Tsuji H, Hattori M, et al. Luminescence properties of Ge implanted SiO_2: Ge and GeO_2: Ge films[J]. Applied Surface Science, 2009, 256(4): 954-957.

Fundamental Study on Auto-Coupled Laser-Electrochemical Co-Machining of Single Crystal Germanium

Wang Chao, Zhu Hao*, Zhang Zhaoyang, Jiang Zixuan, Du Wenwu, Zhang Min
School of Mechanical Engineering, Jiangsu University, Zhenjiang 212013, *Jiangsu, China*

Abstract

Objective Microfabrication of semiconductors is crucial because semiconductor materials are extensively employed in solar cells, microelectronic machinery, optical components, etc. Due to the characteristics of semiconductor materials, including a fast increase in electrical conductivity with temperature, and high hardness and brittleness, traditional mechanical processing has been unable to meet the demands of microfabrication. Simple electrochemical processing has low processing efficiency, severe stray corrosion, environmental pollution from electrolyte solutions, and other challenges. Because the laser has the benefits of high precision and strong domain fixation to produce thermal impact on materials and the integration of electrochemical processing has the benefit to eliminate microcracks and heat-affected zones, the laser and electrochemical machining can be combined to produce good surface processing quality. Thus, the single-crystal germanium is employed as the experimental material, and a neutral and non-polluting $NaNO_3$ electrolyte is employed to perform backward laser-controlled electrolytic processing to confirm the processing mechanism's feasibility, and on this basis, a auto-coupled laser-electrochemical co-machining approach is employed to perform experimental research on micro grooving of single-crystal germanium materials.

Methods In this research, an experimental investigation of single-crystal germanium through auto-coupled laser-electrochemical co-machining is performed. First, a scanning electron microscope is employed to observe the processing morphological characteristic, an energy spectrometer is employed to detect the elements and their occupancy, a confocal microscope is employed to obtain 3D morphology, and a Raman spectrometer is employed to examine the residue composition on the dimple and record the current changes during processing. To examine the dimple's depth, entrance diameter, removal volume, and sidewall taper produced by processing in terms of both heat and mass transfer. Based on this, the experimental research of microgrooves is conducted using laser-electrochemical co-machining to investigate the morphological characteristics of microgrooves under the combined laser and laser-electrochemical processing and to examine the trends in microgroove width and depth under the auto-coupled hybrid laser electrochemical machining.

Results and Discussions Auto-coupled laser-electrochemical machining is employed to achieve non-ablation on the upper surface and electrolytic micro-dimples on the lower surface to confirm the processing mechanism. The benefit of this approach is that the irradiation position of the incident laser corresponds to the electrolytic dimple's position, and no

special cathode design is needed for the automatic coupling process. The obtained electrolytic dimples are free of microcracks and heat-affected zones, which are typical characteristics of electrolytic processing (Fig. 5). Isolated and non-dense oxide GeO_2 attached to the machined surface can hinder the electrolytic processing and influence the surface quality of single-crystal germanium (Figs. 6 and 7). The current variation's trend demonstrates that the large change in current between the laser beam's withdrawal and the addition of the processing beam is attributed to the localized increase of the conductivity of single crystal germanium by laser irradiation. The processing results demonstrate that the maximum entrance diameter, depth, removal volume, and sidewall taper are obtained at the offset distance of 7–9 mm. This finding may be related to the impact of offset distance on both aspects of heat and mass transfer. For the small offset distance, the cooling impact is not conducive to material reduction, and is conducive to the discharge of processing products and suppression of concentration polarization. For the large offset distance, the cooling impact is weak, but the product discharge ability is also reduced, both of which contradict each other and jointly determine the processing process and findings (Fig. 8). Based on this, the characteristics of microgroove morphologies processed by various processing approaches are investigated, and it is concluded that auto-coupled laser-electrochemical co-processing can eliminate the defects including recast layer and scatters caused on the surface, and obtain better microgroove morphology (Figs. 11 and 12). Meanwhile, this AHLECM is employed to investigate the impacts of various processing voltages on the processing findings, and it is found that the microgroove's width and depth gradually widen and deepen with the increase of used voltage (Table 1).

Conclusions It is proposed that laser irradiation can cause a fixed-domain conductive channel within the material, therefore obtaining the processing of single-crystal germanium through auto-coupled laser-electrochemical co-machining. When a neutral sodium nitrate solution is employed as the electrolyte and a horizontal copper sheet is employed as the cathode, the laser irradiation on the upper surface can generate fixed-domain electrolysis on the backside of single-crystal germanium to produce micro-dimple. The offset distance's effect on the dimple morphology is studied. The maximum processing current, dimple diameter and depth, sidewall taper, and removal volume all increase first and then decrease with the increase of offset distance. Their turning points occur at the offset distance of 7–9 mm, and the possible effects generated by various offset distances are examined in terms of heat and mass transfer. By linking laser etching and electrochemical dissolution at the same processing position, the auto-coupled laser-electrochemical co-processing can be achieved, and the preliminary experimental research of microgrooves is conducted. The microgrooves' structural and morphological characteristics are examined, and the processing voltage's influence rules on the microgroove dimensions are investigated. It is found that the microgroove's depth and width increase as the processing voltage increases, which demonstrates that electrochemical dissolution is the crucial phenomenon in the process of auto-coupled laser-electrochemical co-machining.

Key words laser technique; auto-coupled co-machining; laser electrolysis; single-crystal germanium; surface morphology